Control of the number of solitons in the fiber laser cavity due to continuous wave injection

D.A. Korobko[a], V.A. Ribenek[a], P.A. Itrin[a], I.S. Panyaev[a], M.V. Pribylov[a] and A.A. Fotiadi[a, b]
[a]Ulyanovsk State University, 42 Leo Tolstoy Street, Ulyanovsk, 432970, Russian Federation
[b]Electromagnetism and Telecommunication Department, University of Mons, Mons, B-7000, Belgium

ABSTRACT

We report on the experimental and numerical studies exploring dynamical processes of soliton birth and annihilation of solitons in the laser ring cavity. The specific purpose of the research is focused on the exact control of the pulse repetition rate of a harmonically mode-locked fiber laser. We have demonstrated that the birth of a new pulse occurs from the soliton background (i.e., from the dispersive waves) through its shaping to the soliton or from the existing pulse through its splitting. The injection of external continuous wave (CW) allows one-by-one change of the number of solitons in the laser cavity thus enabling the fine-tuning of the pulse repetition rate. We present new experimental observations of the laser transition dynamics associated with the changes of the soliton numbers and give clear insight into the possible physical mechanisms responsible for these effects.

1. INTRODUCTION

Passively mode-locked fiber lasers have become a deserving alternative to semiconductor and solid-state lasers ensuring reliability, compactness, convenient output and single-mode beam quality inherent to fiber lasers. Soliton fiber lasers being in focus of multiple studies for a few decades have proven to be reliable sources of sub-picosecond pulses. Depending on a comprehensive interaction via nonlinearity, dispersion, gain and loss, various multi-pulse states such as soliton molecules and crystals, pulse bunches, noise-like pulses can be formed in the laser cavity making the fiber lasers to be a versatile platform for studies of dissipative system with complex dynamics [1-10]. A special multi-pulse regime of harmonic mode-locking (HML) enabling uniform distribution of multiple solitons in the cavity is used in a wide range of practical applications [11-15].

To describe the physical mechanisms responsible for laser operation in different multi-pulse regimes the specific features of the laser dynamics associated with pulse interaction within the laser cavity, transitions between different laser steady-states, soliton birth and annihilation have been intensively studied [16, 17]. The role of background radiation as a mediator providing the equalizing interaction between pulses has been intensively discussed in this context [18-22]. Recent studies of the transit processes in the HML laser have confirmed an importance of the pulse interaction with the background radiation in the build-up or annihilation of soliton pulses [23, 24]. In our direct experiment, we have studied the effect of the CW injected into the laser cavity from an external narrow-band laser source on the HML laser operation. We demonstrate that under a proper pump power adjustment the optical injection could trigger a complex transition process in the laser cavity resulting in the birth or annihilation of individual solitons. The effect exhibits a strong resonant dependence on the wavelength of the injected CW and makes no impact on other laser performance characteristics. We have also explored a possible application of the observed effect for precise tuning of the HML laser pulse repetition rate (PRR) [23]. Commonly, with perfect adjustment of the pump power, the number of solitons in the HML laser cavity could be changed simultaneously by a large number. It is known as a part of the hysteresis effects typical for soliton lasers [25, 26]. Surprisingly, the technique based on the CW injection enables PRR tuning with an elementary step equal to the fundamental frequency. However, the physical mechanisms underlying these laser properties have not been considered yet. In this work, we have performed new studies on dynamical processes in a HML fiber laser, in particular, considering the birth and annihilation of individual solitons in the laser ring cavity. We report on new experimental findings in the laser transition dynamics associated with the changes of numbers of solitons inside the cavity and propose numerical model of the laser operation exploring the possible physical mechanisms responsible for these effects.

Nonlinear Optics and its Applications 2024, edited by John M. Dudley, Anna C. Peacock, Birgit Stiller, Giovanna Tissoni, Proc. of SPIE Vol. 13004, 130040X
 · 0277-786X · doi: 10.1117/12.3022139

2. EXPERIMENT

In this section, we describe the results of our recent experiments demonstrating the effects of birth and annihilation of the solitons in the laser cavity triggered by the resonant injection of an external CW light. The experimental configuration of an Er-doped soliton nonlinear polarization evolution (NPE) mode-locked fiber ring laser shown in Fig. 1 is not so different from one used in Ref. [23]. The laser cavity consists of two types of fibers: 0.8 m length of heavily erbium-doped fiber (EDF) with normal dispersion (- 48 ps/nm /km) and standard single mode fiber (SMF-28) with anomalous dispersion (17 ps/nm/km). The total length of the laser cavity of 20.5 m corresponds to the fundamental PRR $f_0 = 13.46\ MHz$. The laser is pumped at 980 nm from two laser diodes specified for maximum power of 500mW.

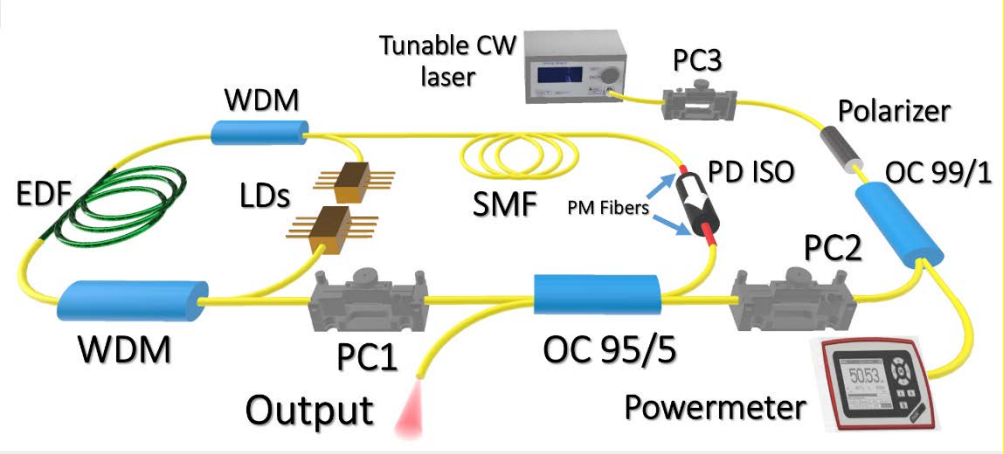

Fig. 1. Experimental HML laser setup.

The light from the external tunable laser source "Yenista T100" is introduced into the ring fiber cavity through the in-line polarization controller PC3, in-line polarizer, 1/99 fiber coupler (OC), polarization controller PC2, and fiber 5/95 coupler. The laser is tunable in the range of 1550-1590 nm and set to operate with the linewidth of ~ 100 kHz and maximal output power of ~ 5 mW. The polarization controller PC3 is used in combination with the in-line polarizer for smooth control of the CW laser power. The polarization controller PC2 is used to control the polarization state of the CW radiation injected into the ring fiber cavity.

Fig. 2 highlights details on the laser operation without optical injection. The laser wavelength is set to λ ~ 1562 nm. At a low pump power level (~50 mW), the laser operates regular pulses with the fundamental frequency f_0 when only a single soliton pulse circulates in the laser cavity. With an increase of the pump power the laser switches to multi-pulse regime. At this stage, an extra delicate adjustment of PC1 regularizes the generated pulses enabling HML laser operation. The laser emits regular pulses with the PRR equal to m pulses per one cavity round trip time, $f_{rep} = mf_0$. In the experiment, the PRR is registered by the RF spectrum analyzer R&S FSP (40GHz). Fig. 2 (a) shows evolution of the average output power and the PRR with the total pump power (both laser diodes contribute equally). Hereinafter, PC1 setting is kept fixed making the presented data completely reproducible. The total pump power is increased up to 1W and then decreased down to ~60 mW. With the maximal pump power of ~1W, the PRR gets ~ 6.75 GHz. Red and blue lines highlight the soliton hysteresis effect reflecting instantaneous PRR changes in cases of increasing and decreasing pump power. The positive or negative PRR jumps $\Delta f_{rep} = \Delta m f_0$ are associated with simultaneous birth or annihilation of Δm solitons. The PRR points match black square points describing the laser output power in Fig.2(a). Analyzing these data, we have concluded that the laser output power is almost a linear function of the laser PRR that allows to estimate the laser energy accounted for a single soliton. It slightly changes from 1.2 pJ at 580 MHz down to 1.1 pJ at 6.5 GHz.

The result of the CW interaction with the laser radiation inside the cavity depends on the wavelength, power and polarization state of the injected light, all adjusted independently. In particular, it is due to the fiber birefringence filter formed in the fiber laser cavity exhibiting a periodic spectral transmittance for radiation. In operation of the laser based on the NPE this filter plays a crucial role. We can expect the fiber birefringence filter to produce a similar effect on the injected CW propagating inside the fiber laser cavity. For better interaction the polarization state of the injected CW has to be adjusted by PC2 to the polarization state of the fiber laser radiation (at least, on average). For this purpose, the CW laser

wavelength is set to be within one of the filter transmission maximum band and then PC2 adjustment is used to get the maximal power of the injected light detected at the HML laser output. After that the PC2 settings are kept fixed over the experiments. This intuitive analysis is in a good agreement with our experimental observations. We have observed that the injection of external CW into the laser cavity operating HML does not affect the laser operation itself but can change the PRR of generated pulses. To get the effect with the HML laser operating at 1562 nm (see, Fig.2), the wavelength of the injected CW laser should be selected within one of two narrow bands (typically <0.2 nm) centered at $\lambda_{1cw} \approx 1557.5\ nm$ (Fig. 2 (b)) and at $\lambda_{2cw} \approx 1572.5\ nm$ (Fig. 2 (c)). These spectral bands become broader (up to ~ 1 nm) with an increase of the CW power. Based on the above, we have concluded that the wavelengths λ_{1cw}, λ_{2cw} are close to the transmittance peaks of the fiber birefringence filter [16] surrounding the laser operation wavelength. Beyond these bands, no effect of the injected CW on the HML laser behavior has been observed (see, Fig.2 (b, c)).

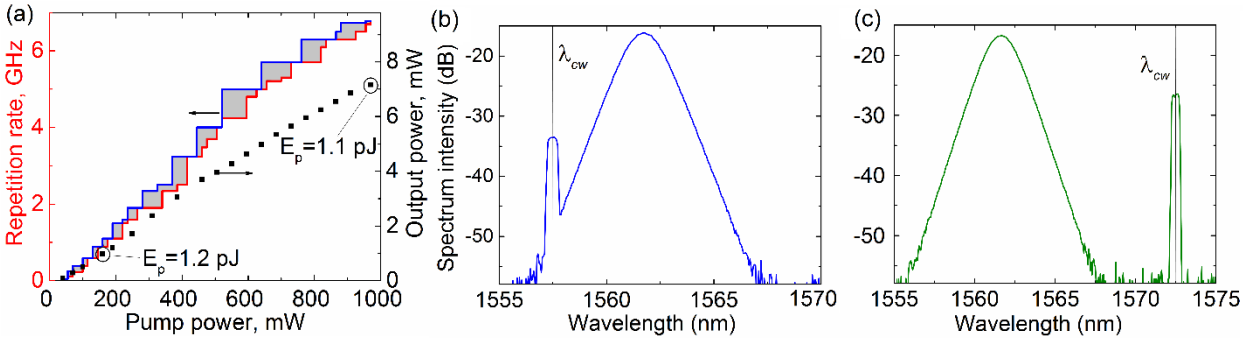

Fig. 2. (a) PRR as functions of the increasing (red line) and decreasing (blue line) pump power. The output power is shown by black squares. In gray areas, PRR can be tuned with the step of f_0. Optical laser spectrum with the CW light injected at λ_{cw1} (b), λ_{cw2} (c).

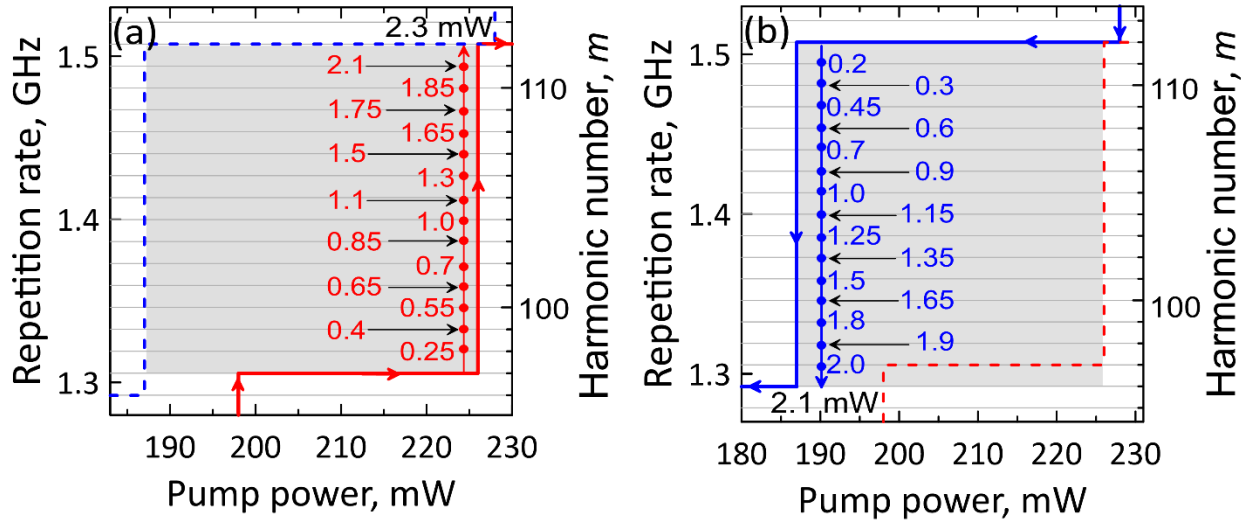

Fig. 3. Fine one-by-one tuning from 97th to 112th (a) and from 112th down to 96th (b) harmonics provided by the gradual increase of the injected CW power from 0 to 2.3 mW (a) and from 0 to 2.1 mW (b).

Commonly, the effect of the injected external CW on the HML laser PRR could be demonstrated as follows. The HML laser emits the regular pulses with the PRR corresponding to the set pump power level. According to Fig.2, only a limited number of the discrete PRRs $f_i^+ = m_i^+ f_0$ and $f_j^- = m_j^- f_0$ are obtainable with increasing and decreasing pump powers, where m_i^+ and m_j^- are the corresponding numbers of solitons in the cavity, respectively, and $i, j = 1, 2...$. Each PRR point f_i^+ or f_j^- is associated with the pump power segment $\left[p_i^+, p_{i+1}^+\right]$ or $\left[p_{j-1}^-, p_j^-\right]$, where the number of pulses in the cavity m_i^+ or m_i^- does not change. The discussed effect can be observed with any initial PRR, but it is more pronounced

at the pump powers, where large PRR jumps occur. In order to demonstrate the effect with the initial PRR of f_i^+ or f_j^- and increasing or decreasing power, we have to set the pump power near the point $p_{i+1}{}^+$ within the interval $\left[p_i^+, p_{i+1}{}^+\right]$ or near the point $p_{j-1}{}^-$ within the interval $\left[p_{j-1}{}^-, p_j^-\right]$, respectively. Then keeping the pump power fixed, we can accurately tune PC3 to increase gradually the CW power injected into the HML laser cavity. Fig. 3 shows the fine-tuning from 97th up to 112th (a) and from 112th down to 96th (b) harmonics. With an increase of the injected power, the number of pulses inside the HML laser cavity (and PRR, correspondingly) increases or decreases one-by-one, until the next stable level of $m_{i+1}{}^+$ or $m_{j-1}{}^-$ shown in Figs. 2(a) is achieved (in Fig.3 $m_{i+1}{}^+ = 112$, $m_{j-1}{}^- = 96$). Importantly, this process could be stopped at any moment by reducing the injected power down to zero. In this case, the HML laser continues to generate pulses with the PRR corresponding to the last transition.

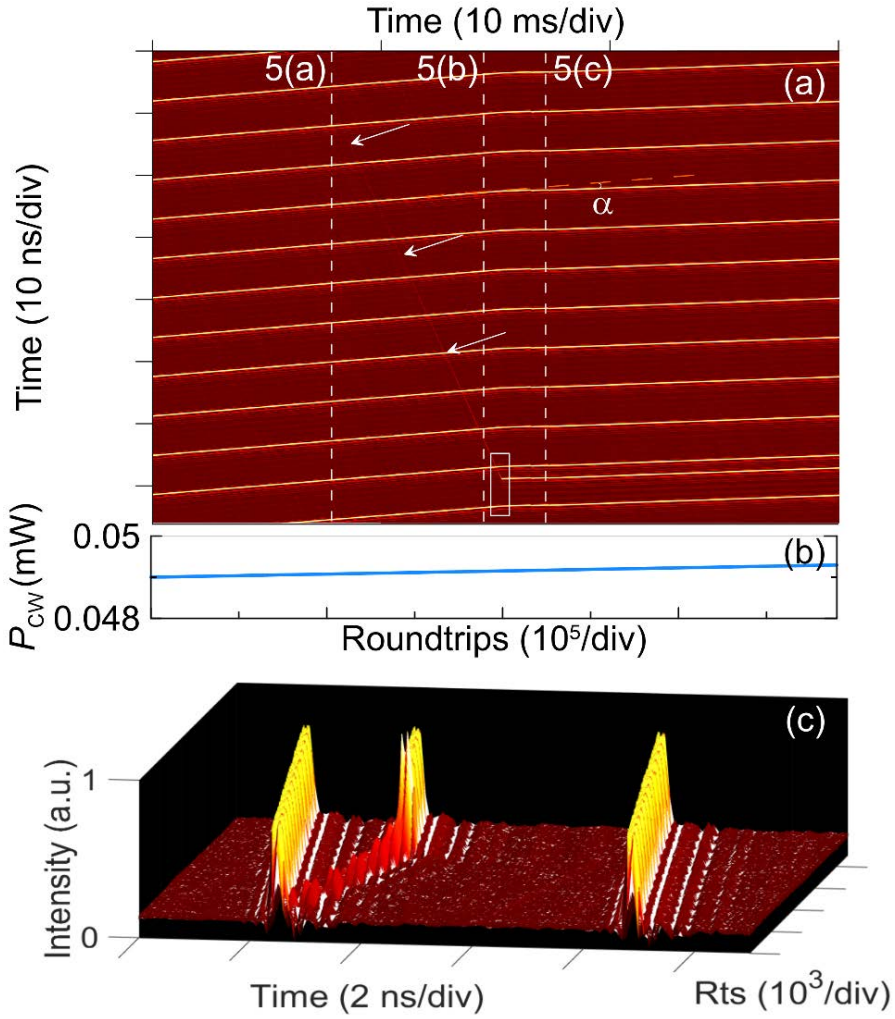

Fig.4. (a) Real-time recording of the transition dynamics from a 12th HML state to the state with 13 pulses in the cavity. Arrows point to the trajectory of the weak background pulse. Dashed lines correspond to temporal profiles (a, b, c) in Fig. 5. Angle α is determined by change of the group velocity after the birth of new soliton. (b) CW power dynamics. (c) Close-up of the area highlighted in (a).

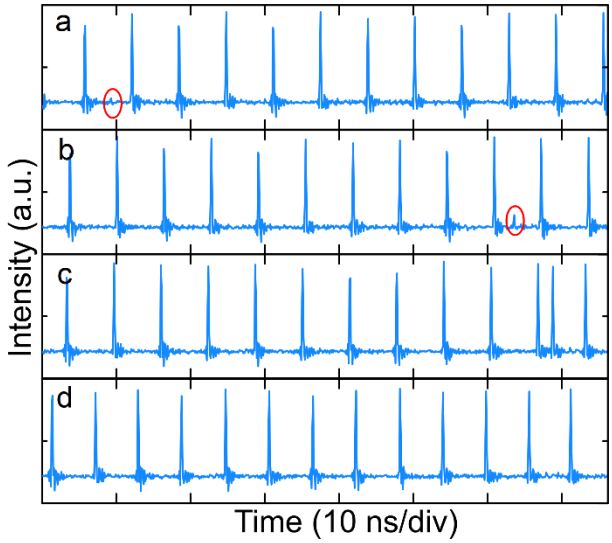

Fig.5. (a), (b), (c) Oscilloscope traces during the new pulse formation process. In (a) and (b) the seed of new pulse is circled. (d) Oscilloscope trace corresponding to the mode-locking on the 13th harmonic of the cavity.

In the next experiment, the real-time transition dynamics of new pulse birth during the CW injection has been captured with a Yokogawa AQ 7750 (4 GHz) oscilloscope. Using the pump power of ~95 mW, the fiber ring laser is set to operate the HML at PRR MHz that corresponds to the 12th harmonic of the fundamental frequency. The CW is injected into the band near , whereas the CW light power is continuously increasing linearly from a minimum value of ~0.01 mW. The pulse train generated by the laser is recorded by the oscilloscope synchronized with the CW rise. At some moment, the birth of a new pulse is registered (Fig. 4) by the oscilloscope that also has managed to record its further evolution. Specifically, new soliton is originated from a weak fluctuation of the dispersive wave (background) neighboring one of the solitons. To become a soliton, the originating pulse first wins the competition with the other background pulses. Then it is amplified in the cavity suffering the soliton shaping through the saturable absorption mechanism. This process is shown in Fig. 5.

The birth of new soliton in the laser cavity affects the velocity the other solitons circulating in the cavity. Real-time recording of the new soliton evolution allows measuring the change of the velocity associated with the birth of new soliton. One can see this effect in Fig.4 (a); the angle α is inversely proportional to the soliton velocity change at the moment of new soliton birth. This observation can be explained recalling the gain depletion and recovery mechanism that provides soliton repulsion inside the cavity [27-31]. As a result, the birth of new soliton is accompanied by redistribution of accumulated energy among all solitons. The energy of each soliton circulating in the cavity decreases leading to simultaneous reduction of their velocity. One can see that the trajectories of all solitons are almost parallel, but not precisely. The gain depletion and recovery mechanism enables their slow equalization resulting in restoration of the HML regime in the laser operating with new PRR. The final harmonic distribution of pulses in the cavity recorded 20 seconds after the new soliton birth is shown in Fig. 5(d).

In the next section, we build the HML laser model and perform numerical simulation of the HML laser dynamics to explore physical mechanisms responsible for the soliton birth and annihilation processes.

3. NUMERICAL MODEL

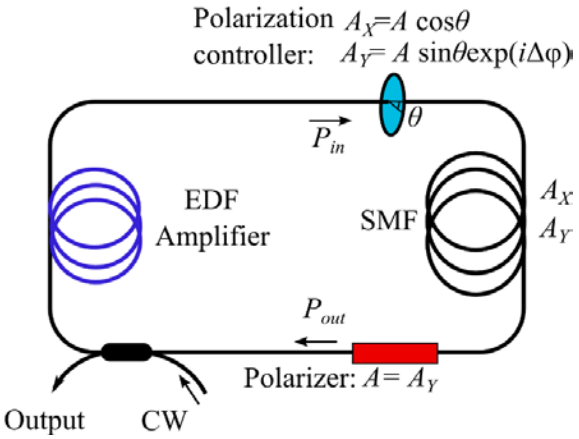

Fig.6. The scheme of laser setup used in simulations.

The configuration of fiber ring laser with CW injection used for numerical analysis is close to the one described earlier [20, 32]. It is depicted schematically in Fig. 6. The configuration comprises a gain fiber (or EDF amplifier), a polarization controller (PC), a piece of passive SMF, a polarizer, and an output coupler. We assume that the light propagating in the gain fiber is linearly polarized, whereas the light propagating in SMF could possess an elliptical polarization. For this reason, a negligibly low fiber birefringence is assigned to the passive fiber and the polarizer is used for modeling the polarization-dependent optical isolator shown in Fig.1.

The light propagation through the laser cavity is described by the nonlinear Schrodinger type equations. An evolution of the optical field amplitude in the gain fiber of length l_a is governed by the generalized NLS equation:

$$\frac{\partial A}{\partial z} - i\frac{\beta_{2g}}{2}\frac{\partial^2 A}{\partial t^2} - i\gamma_g |A|^2 A = \frac{gA}{2} + \frac{g}{2\Omega_g^2}\frac{\partial^2 A}{\partial t^2}, \qquad (1)$$

where, A is the complex amplitude of the linearly polarized electric field in the gain fiber, z is the coordinate along the fiber, β_{2g} is the group velocity dispersion, and γ_g is the Kerr nonlinearity of the gain fiber. The gain spectral filtering is centered at λ_0 and employed in parabolic approximation with the FWHM gain line bandwidth Ω_g. The saturated gain factor g

$$g = g_0\left(1+\frac{E_f}{E_g}\right)^{-1} = g_0\left(1+\frac{1}{E_g}\int_0^{\tau_{win}} |A(z,t)|^2\, dt\right)^{-1}, \qquad (2)$$

is determined by the small signal gain g_0, saturation energy E_g and total energy in the cavity E_f. τ_{win} is the width of the simulation window.

The light propagation in the passive SMF of length l_{SMF} is described by the two coupled nonlinear Schrodinger equations:

$$\begin{aligned}
&\frac{\partial A_X}{\partial z} - i\frac{\beta_2}{2}\frac{\partial^2 A_X}{\partial t^2} - i\gamma\left(|A_X|^2 + \frac{2}{3}|A_Y|^2\right)A_X - \frac{i}{3}\gamma A_X^* A_Y^2 = 0,\\
&\frac{\partial A_Y}{\partial z} - i\frac{\beta_2}{2}\frac{\partial^2 A_Y}{\partial t^2} - i\gamma\left(|A_Y|^2 + \frac{2}{3}|A_X|^2\right)A_Y - \frac{i}{3}\gamma A_Y^* A_X^2 = 0,
\end{aligned} \qquad (3)$$

where A_X and A_Y are the field amplitudes of two polarization components. The effects of cross-modulation and four-wave mixing are taken into account by the third and fourth terms in Eq.3. To avoid the effects associated with the fiber

cavity inhomogeneity, the gain fiber and the SMF are assumed to have the same nonlinearity $\gamma_g = \gamma$ and dispersion $\beta_{2g} = \beta_2$.

We assume that the light propagating in the gain fiber is linearly polarized, whereas the light propagating in SMF possesses an elliptical polarization (see, Fig.6). With this assumption the polarization state at the SMF input is determined by the polarization controller as $A_X = A\cos\theta$, $A_Y = A\sin\theta\exp(i\Delta\varphi)$, where θ is the angle between the polarization direction of the input light and the fast axis of the SMF and $\Delta\varphi$ is the phase difference between two polarizations. The block combining the PC, SMF and the polarizer operates as a nonlinear "absorber". Its transmission involving NPE is a saturating function of the input signal power $|A|^2$ that at a certain set of parameters ensures the laser mode-locking, providing the generation of an ultrashort pulse. All the linear losses experienced by the signal inside the cavity are taken into account as the local losses in the output coupler described by its power transmission coefficient $\rho^2 : A' = \rho A$.

The CW injection at the kth roundtrip through the cavity is taken into account by the relations

$$A_{CW}(t,k) = \sqrt{p_{CW}}\exp\left(i\left(\omega_{CW}t + \beta_2\omega_{CW}^2(l_{SMF}+l_a)(k-1)/2 + \Delta\varphi(k-1)\right)\right), \qquad (4a)$$

$$A(t,k) = A(t,k-1) + A_{CW}(t,k)\exp(i\Delta\phi), \qquad (4b)$$

where p_{CW} is the CW power inside the cavity, ω_{CW} is the CW frequency. Condition (4a) in the linear approximation describes the change of the CW phase after a complete roundtrip in the cavity and condition (4b) describes the change of the amplitude A in each roundtrip due to the CW injection. The CW phase jump per in each roundtrip $\Delta\phi$ is caused by the noncoincidence of the ω_{CW} with the cavity mode. At $\Delta\phi = 0$, a precise coincidence of the CW with the closest cavity mode is observed. Equations (1-4) with the boundary conditions in accordance with Fig. 6 have been numerically simulated employing the split-step Fourier method. The cavity parameters used for calculations are typical for the considered type of the HML lasers and listed in Table 1.

Table 1. The system parameters used for calculations

Parameter	Value	Parameter	Value
γ (W-1 m-1)	0.0033	Ω_g (ps-1)	3.5
β_2 (ps2m-1)	-0.018	g_0 (m-1)	0.2
θ	$(\pi+1)/4$	l_{SMF} (m)	10
$\Delta\varphi$	$\pi/4$	l_a (m)	2.5
ρ	0.95	τ_{win} (ps)	30.72-61.44

4. SIMULATION OF A SYSTEM WITHOUT CW INJECTION

Without injection of the external CW component, the considered laser model describes dynamics of a soliton fiber laser. We explore the laser system dynamics established after ~2500 roundtrips in the cavity. Since the saturation energy E_g is proportional to the pumping strength [25], the increasing E_g corresponds to the increasing pump power in the experiments. In simulations, the self-started mode locking is achievable at $E_g > 3$ pJ. Similar to the experiment, an increase of E_g leads to an increase of the pulse energy and, as a result, to the birth of a new pulse. And vice versa, a decrease of E_g causes a decrease of the pulse energy resulting in annihilation of the soliton. In this section, we explore the specific features of this process in the region of soliton hysteresis for increasing and decreasing E_g.

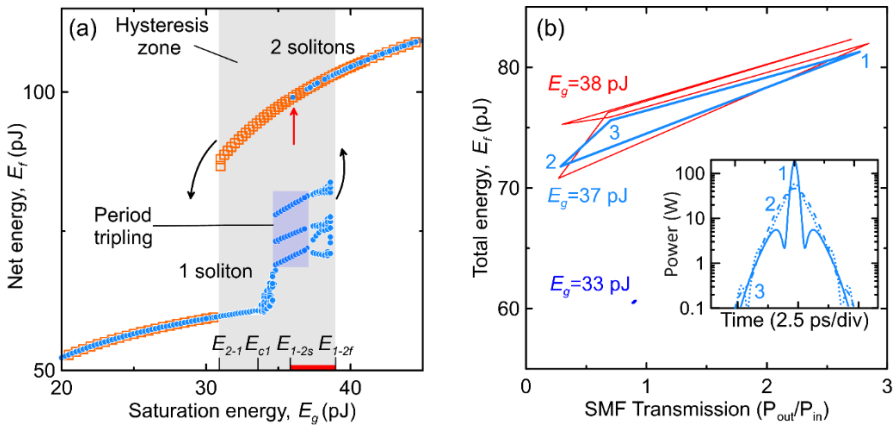

Fig.7. (a) The net cavity energy in the laser system without CW injection as a function of E_g in the range close to the transition area between the single- and double- soliton steady-states. The blue circles and orange squares describe the system with a single- and double- soliton initial state, respectively. (b) The net cavity energy changes in the system with the initial single-soliton steady-state and the corresponding SMF transmission at different E_g. Inset: the shape of the laser pulse possessing period-tripling ($E_g = 37$ pJ).

Fig. 7 (a) presents the data obtained for 10 consequent roundtrips (after ~2500 roundtrips in the cavity) using two types of the initial system states. It depicts the net cavity energy $E_f = \int |A|^2 dt$ as a function of E_g. In the first case (blue circles), the initial conditions are simulated as a single-soliton pulse combined with a low-amplitude noise component simulated as a Gaussian stochastic process. Following this branch from the low to high E_g values, one can see that the energy E_f increases with the saturation energy E_g passing several specific regions. Until reaching the first critical point $E_g = E_{c1} \approx 34$ pJ the cavity energy E_f is a single-valued function changing monotonically with E_g. At each E_g it characterizes the steady state soliton that does not change with the cavity roundtrips. Above the first critical point E_{c1} the conversion of the pump to the soliton energy increases. In this range the steady state solution is no longer supported and the soliton energy changes every roundtrip resulting in broadening of the considered curve due to multiple values of the net cavity energy recorded at the same E_g. Within the saturation energy range $34\text{pJ} < E_g < 38.5$, the character of the soliton energy instability changes from low-amplitude fluctuations to regular pulsations, highlighting the tripling of the soliton period, and then to chaotic pulse perturbations. This system behavior is typical for nonlinear dynamic systems performing transition from a stable to a chaotic state [33-37].

Fig. 7(b) illustrates the pulsating soliton dynamics within the transition domain by comparing the net cavity energy E_f and peak cavity transmission coefficient P_{out}/P_{in} changes recorded for several roundtrips at different E_g values. The peak power ratio P_{out}/P_{in} is determined by the NPE in the SMF. Physically, the soliton pulsations occur when the pulse peak power exceeds the power range enabling the positive cavity feedback provided by the NPE in the cavity fiber [26]. In this case the peak power ratio changes with roundtrips (even at a fixed E_g) thus affecting the shape of the propagating pulse. With the increasing pump, the steady single-pulse state (shown at $E_g = 33$ pJ) is replaced by the pulsating state with the soliton period equal to three roundtrips (shown at $E_g = 37$ pJ). A salient trait of such laser system state is a broad pulse pedestal, like shown in the inset of Fig.7 (b). One can see that in this domain very small changes of the pulse pedestal could cause drastic changes of the pulse peak power. A further pumping increase leads to chaotization of pulsations (shown at $E_g = 38$ pJ) resulting in birth of a new soliton, i.e. transition of the system to a double-soliton steady state.

The detailed analysis of the numerical simulations has explored that the birth of a new pulse occurs from the soliton background (i.e., from the dispersive waves) through its shaping to the soliton or from the existing pulse through its splitting. The birth of a new soliton is found to be a probability process that relies on the current parameters of the noise component simulated as a Gaussian stochastic process. Over the ensemble of similar simulations, the probability of the

second soliton birth exhibits a threshold dependence on E_g. In fact, there are two thresholds associated with this process. When the saturation energy E_g reaches the first threshold $E_{1-2s} \approx 36$ pJ (red arrow in Fig. 7(a)) the transition to the double-pulse state may already occur, but the probability of this process is rather low. With an increase of the saturation power E_g the probability of the second pulse generation increases and reaches 100% at the second threshold $E_{1-2f} \approx 39$ pJ. At $E_g > E_{1-2f}$ the system definitely transfers from a single-pulse to a double-pulse steady state independently of the current realization of the stochastic noise component. The probability of the soliton birth as a function of E_g is shown in Fig. 8.

Similar numerical calculations have been applied to explore the pulse annihilation process. The initial conditions are simulated as a double-soliton combined with a low-amplitude noise component simulated as a Gaussian stochastic process. The simulation results are shown in Fig. 7(a) by orange squares. Following this branch from the high to low E_g values, one can see that the soliton energy E_f decreases monotonically with the decreasing saturation energy E_g until reaching the threshold value at $E_{2-1} \approx 31$ pJ. In contrast to the soliton birth process, the pulse annihilation process exhibits only one threshold. At each E_g above this point the soliton energy E_f characterizes the double-soliton steady-state that does not change with the cavity roundtrips. Once the decreasing laser saturation energy E_g reaches this threshold, the system is mandatory converted from the double-soliton steady-state to the single-soliton laser steady-state avoiding any intermediate transition states. In other words, the soliton annihilation process does not rely on the current parameters of the noise component and exhibits 100% probability as soon as the saturation energy lower than the threshold value E_{2-1} is reached. In this sense, the soliton annihilation is similar to the soliton birth process taking place above the second threshold E_{1-2f}. Indeed, below the second threshold E_{1-2f}, in the range between the first and second threshold $E_{1-2s} < E_g < E_{1-2f}$, the system transition from the single-soliton steady-state to the double-soliton steady-state depends on the current parameters of the stochastic noise component and its probability increases from 0 to 100% when E_g increases within this range. However, the soliton birth process becomes independent of the current parameters of the noise component and exhibits 100% probability once the saturation energy exceeds the threshold value E_{1-2f}.

5. SIMULATION OF PULSE BIRTH/ANNIHILATION IN THE SYSTEM WITH INJECTED CW

In this section we apply the proposed laser model to explore the effect of the CW injection on the single soliton birth/annihilation processes in the HML laser cavity. We have performed a series of simulations similar to those reported in the previous section to explore the laser system states established after ~2500 roundtrips in the cavity. For simplicity, we restrict our consideration to the simplest case of $\omega_{CW} = 0$, when the CW injection wavelength coincides with the active fiber gain line maximum and soliton laser spectrum central wavelength. In this case, the effect of the CW injection on the laser system dynamics is maximal and controllable by only three system parameters that are the laser saturation energy E_g, CW light power p_{CW}, and its phase $\Delta\phi$. The CW light power p_{CW} is evaluated in units normalized to $p_0 = E_g / \tau_{win}$, where τ_{win} is the simulation window size.

The effect of the CW injection on the soliton birth process is demonstrated in Fig. 8. The initial single-soliton laser state is simulated as a superposition of a soliton pulse with a low-amplitude noise modeled as a Gaussian stochastic process. Fig. 8 depicts the probability of the system transition to the double-soliton steady state induced by the CW light injection as a function of the laser saturation energy E_g at different values of the CW light power p_{CW} and phase $\Delta\phi$ (a-c). To collect these data, the simulations have been repeated 50 times for each set of the parameters (E_g, p_{CW}, $\Delta\phi$). At $p_{CW} = 0$, the presented data depict the probability of the second soliton birth through the process described in the previous section. This process is associated with the complex dynamics of the background pulsations in the cavity exhibiting stochastic behavior. We have already shown that in the pulsation state even slight changes of the pulse background can lead to drastic changes of the pulse peak power. The injected CW ($p_{CW} \neq 0$) affects the background level thus affecting the original saturation energy E_g ranges (determined by the critical points E_P, E_{1-2s}, E_{1-2f}) established without the CW injection, i.e., at $p_{CW} = 0$. One can see that with $\Delta\phi$ value varied between $\pi/4$ and $\pi/2$ the first and second threshold points E_{1-2s}, E_{1-2f} limiting the ranges with a non-zero and 100% probability of the system transition to the single-soliton steady-

state, respectively, shift towards the first critical point E_{c1}. The value of this shift is determined by the CW power p_{CW} and so the effect is more pronounced for the maximal p_{CW} values. At high CW injection powers p_{CW} both threshold points E_{1-2s}, E_{1-2f} move towards the first critical point $E_{c1} = 34$ pJ, merge, but never overtake it. In other words, the laser system transition to the single- soliton steady-state under CW injection always occurs within the range of the saturation energy E_g where the system without CW injection exhibits the pulsating dynamics. The transition to the double-soliton steady state never occurs at the saturation energy below the first critical point E_{c1}. The role of the CW phase $\Delta\phi$ in this process seems to be rather trivial. At $\Delta\phi \neq 0$, the injected light perturbates the soliton background resulting in the corresponding changes of the pulse peak power. We suggest that such perturbations could trigger the laser system transition to the double-soliton state. In any case, no specific regularities have been found for the effect of the phase detuning $\Delta\phi \neq 0$ on the laser system dynamics. For comparison, the CW injection at $\Delta\phi = 0$ produces a stabilization effect of the laser system. It forms a uniform pulse background causing a decrease of the cavity gain g. As a result, the laser single-soliton steady-state could not be changed by any combination of the saturation energy and CW power selected from the whole available for simulation range.

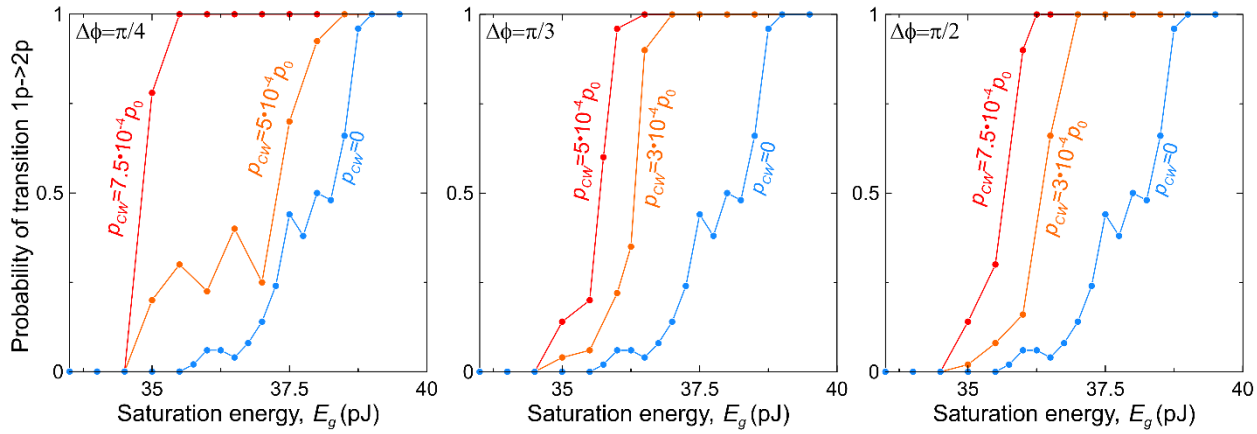

Fig. 8. Probability of the system transition from the single-soliton steady-state to the double-soliton steady-state (soliton birth process) caused by the CW injection as a function of the saturation energy E_g and at different values of p_{CW} and $\Delta\phi$.

It is worth noting that with the selection of the E_g values in the range between E_{c1} and E_{1-2s} the laser system transition process induced by the CW injection is unidirectional. The CW injection converts the system from single-soliton to double-soliton steady-state but does not support the opposite transition. When after the transition the CW power is switched-off, the laser system remains in the double-soliton steady-state. Therefore, this effect can be employed for controllable birth of solitons in the cavity.

Fig. 9 demonstrates the effect of the CW injection on the soliton annihilation process. The initial double-soliton laser state is simulated as a superposition of two equidistant soliton pulses and low-amplitude Gaussian noise. Fig. 9 depicts the net cavity energy E_f as a function of the CW power p_{CW} for different values of the phase $\Delta\phi$ (a-d) and two values of the laser saturation energy $E_g = 32$ pJ (red) and $E_g = 32.5$ pJ (blue) taken within the transition range shown in Fig.7(a).

To collect these data, the simulations have been repeated five times for each set of parameters (E_g, p_{CW}, $\Delta\phi$). One can see that the results related to the same series do not almost differ from each other. It means that the selected set of parameters completely determinates the further laser system evolution: either maintaining the initial two-soliton steady-state or transition to the single-soliton steady-state. The stochastic laser noise makes a minor contribution to these deterministic processes. One can see that for all considered cases of E_g and $\Delta\phi$ the transition to the single-soliton steady-state is not achievable without the CW injection (i.e., with $p_{CW} = 0$).

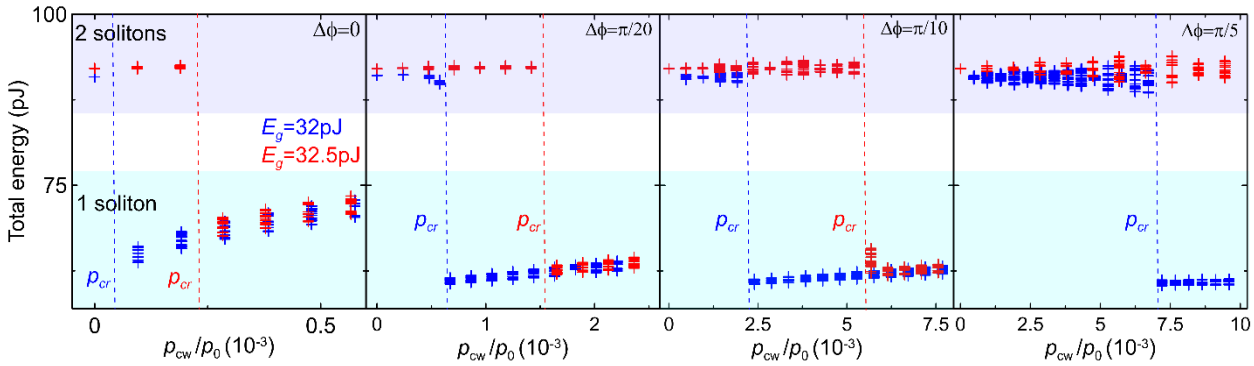

Fig. 9. The system transition from the double-soliton steady-state to the single-soliton steady-state (soliton annihilation process) caused by the CW injection at the given p_{CW} and $\Delta\phi$. The saturation energy is $E_g = 32$ pJ (blue crosses), $E_g = 32.5$ pJ (red crosses). The symbols corresponding to the same p_{CW} value show E_f for 10 consequent roundtrips to demonstrate the unstable pulsating state.

To annihilate soliton the injected CW light power p_{CW} should be set above some critical power p_{cr}. When $E_g \to E_{2-1}$, the critical value $p_{cr} \to 0$ and it increases rapidly with increasing $E_g > E_{2-1}$. On the other hand, p_{cr} is minimal at $\Delta\phi = 0$, i.e., when the CW injection is resonant with the laser cavity ensuring the highest background level available in the cavity. High background level provides an additional saturation to the cavity gain g. Thus, we can conclude that the pulse annihilation occurs due to the saturation of the cavity gain g caused by the CW injection below the critical level. With the $\Delta\phi$ detuning from the cavity resonance, the level of the total energy in the cavity decreases and the critical CW power p_{cr} should be increased to enable the same decrease of the cavity gain g. It is worth noting that with the selection of the E_g values near the threshold E_{2-1} the process induced by the CW injection is unidirectional. The CW injection converts the system from two-soliton to single-soliton steady-state but does not support the opposite transition. When after the transition the CW power is switched-off, the laser system remains in the single-soliton steady-state. Therefore, this effect can be employed for controllable annihilation of solitons in the cavity.

6. DISCUSSION AND CONCLUSIONS

In the experiment with a ring fiber HML laser we have observed the hysteresis in the dependence of the laser PRR on the pump power. Up to the maximum PRR of ~6.75 GHz the dependence possesses typical soliton hysteresis areas with the PRR jumps of hundreds of MHz corresponding to the simultaneous birth/annihilation of tens of pulses in the cavity. Using the CW injection into the cavity, we are able to change the number of solitons in the cavity. The effect is observed near critical pump power values corresponding to the PRR jumps. A gradual increase of the CW power enables one-by-one change of the soliton numbers circulating in the cavity. Real-time recording of the soliton train has revealed that the birth of new soliton occurs from a weak soliton background instability through its further amplification and soliton shaping. To explain the observed effects, a series of numerical experiments have been performed to explore the birth/annihilation mechanisms in a fiber laser cavity.

The reported numerical simulations clarify the role of the CW injection in the induced laser system transitions within the grey area shown in Fig. 2 (a). Although the numerical simulations have been performed for the elementary transitions between single- and double- soliton steady-states, it clarifies the very mechanisms responsible for up- and down-conversions in the fiber laser system in general. Importantly, our simulations have revealed that the injected CW enables a strongly dosed effect on the laser system, while the dosage could be strongly controlled by the injection laser power p_{CW}. It is true for both soliton-birth and soliton-annihilation effects, although they rely on rather different physical mechanisms.

We have demonstrated that the birth of a new pulse occurs from the soliton background (i.e., from the dispersive waves) through its shaping to the soliton or from the existing pulse through its splitting [26]. It is found to be a probability process that relies on the current parameters of the noise component that could produce a specific perturbation of the background radiation triggering the birth of new soliton. Over the ensemble of similar simulations, the probability of the second soliton

birth exhibits a threshold dependence on E_g enabling a specific range of the saturation energies E_g (between two thresholds E_{1-2s} and E_{1-2f}), where the birth of new soliton can occur. The injection of the CW light at $\Delta\phi \neq 0$ affects the background level in the laser cavity causing a shift of this $\left[E_{1-2s}, E_{1-2f}\right]$ range towards lower energies thus enabling the process of new soliton generation at lower E_g. Importantly, the displacement of the range could be completely controlled by the CW power. This mechanism could be applied for interpretation of the soliton generation effect observed in the experiment. In accordance with the experiment before the CW injection the laser system operates a number of solitons in steady-state and the saturation power E_g is set near the first transition threshold. Such initial conditions ensure steady-state laser operation, i.e., the probability of new soliton birth is zero. The gradual increase of the CW light power shifts the first transition threshold towards lower energies enabling the controllable increase of the probability of new soliton generation. It allows to control generation of new solitons one-by-one up to the maximal value available in the selected hysteresis area.

We have demonstrated as well that the annihilation of an existing soliton pulse occurs due to a decrease of the net cavity saturated gain value below the critical value thus preventing positive feedback in the cavity. Before the CW injection the laser system operates a number of solitons in steady-state and the saturation power E_g is set near the transition threshold. The CW injection increases the background level thus affecting the cavity saturated gain. The gradual increase of the CW power at $\Delta\phi \neq 0$ provides dosed control of the saturation gain in the cavity thus enabling annihilation of solitons one-by-one down to the minimal value available in the selected hysteresis area.

In conclusion, the soliton birth/annihilation processes in the cavity of a soliton fiber laser have been studied experimentally and numerically. It has been demonstrated that the CW injection allows a precise control of the number of solitons. This effect relies on the strongly dosed CW power injection into the laser system. Depending on the current pump power the CW injection causes either impact on the soliton background thus stimulating the birth of new soliton or reduction of the saturated gain in the laser cavity resulting in one soliton annihilation. We believe that our findings offer important insights into the transient HML laser dynamics associated with the birth and annihilation of solitons, which are crucial for the HML laser design and optimization [38-40].

The work is supported by the Russian Science Foundation (grant # 23-79-30017).

REFERENCES

[1] Amrani, F., Haboucha, A., Salhi, M., Leblond, H., Komarov, A., & Sanchez, F., "Dissipative solitons compounds in a fiber laser. Analogy with the states of the matter," Applied Physics B, 99(1), 107-114 (2010).
[2] Korobko, D. A., Gumenyuk, R., Zolotovskii, I. O., & Okhotnikov, O. G., "Multisoliton complexes in fiber lasers," Optical Fiber Technology, 20(6), 593-609 (2014).
[3] Gui, L., Wang, P., Ding, Y., Zhao, K., Bao, C., Xiao, X., & Yang, C., "Soliton molecules and multisoliton states in ultrafast fibre lasers: intrinsic complexes in dissipative systems," Applied Sciences, 8(2), 201 (2018).
[4] Voropaev, V., Donodin, A., Voronets, A., Vlasov, D., Lazarev, V., Tarabrin, M., & Krylov, A., "Generation of multi-solitons and noise-like pulses in a high-powered thulium-doped all-fiber ring oscillator. Scientific Reports, 9(1), 1-11 (2019).
[5] Gumenyuk, R., Korobko D.A., Zolotovsky, I. O. and Okhotnikov, O. G., "Role of cavity dispersion on soliton grouping in a fiber lasers," Optics Express 22(2), 1896 (2014).
[6] Sanchez, F., Grelu, P., Leblond, H., Komarov, A., Komarov, K., Salhi, M.,& Chouli, S., "Manipulating dissipative soliton ensembles in passively mode-locked fiber lasers," Optical Fiber Technology, 20(6), 562-574 (2014).
[7] Rissanen, J., Korobko, D. A., Zolotovsky, I. O., Melkumov, M., Khopin, V. F. and Gumenyuk, R., "Infiltrated bunch of solitons in Bi-doped frequency-shifted feedback fibre laser operated at 1450 nm," Scientific Reports 7(1) (2017).
[8] Dai, L., Huang, Z., Huang, Q., Chen, Z., Rozhin, A., Sergeyev, S., Araimi, M. A. and Mou, C., "Carbon nanotube mode-locked fiber lasers: recent progress and perspectives," Nanophotonics 10(2), 749–775 (2020).
[9] Song, Y., Shi, X., Wu, C., Tang, D., & Zhang, H., "Recent progress of study on optical solitons in fiber lasers," Applied Physics Reviews, 6(2) (2019).
[10] Yu, Y., Li, B., Wei, X., Xu, Y., Tsia, K. K., & Wong, K. K., "Spectral-temporal dynamics of multipulse mode-locking," Applied physics letters, 110(20) (2017).

[11] Lecaplain, C., & Grelu, P. (2013). Multi-gigahertz repetition-rate-selectable passive harmonic mode locking of a fiber laser. Optics express, 21(9), 10897-10902.
[12] Ribenek, V. A., Korobko, D. A., Fotiadi, A. A., & Taylor, J. R.,. "Supermode noise mitigation and repetition rate control in a harmonic mode-locked fiber laser implemented through the pulse train interaction with co-lased CW radiation," Optics letters, 47(19), 5236-5239 (2022).
[13] Liu, X., & Pang, M. (2019). Revealing the buildup dynamics of harmonic mode-locking states in ultrafast lasers. Laser & Photonics Reviews, 13(9), 1800333.
[14] Gumenyuk, R. V., Korobko, D. A., & Zolotovskii, I. O., "Stabilization of passive harmonic mode locking in a fiber ring laser," Optics Letters, 45(1), 184-187 (2020).
[15] Korobko, D. A., Ribenek, V. A., Itrin, P. A., Stoliarov, D. A., & Fotiadi, A. A., "Polarization maintaining harmonically mode-locked fiber laser with suppressed supermode noise due to continuous wave injection," Optics & Laser Technology, 162, 109284 (2023).
[16] Liu, X., & Cui, Y., "Revealing the behavior of soliton buildup in a mode-locked laser," Advanced Photonics, 1(1), 016003 (2019).
[17] Zeng, J., and Sander, M.Y., "Real-time transition dynamics between multi-pulsing states in a mode-locked fiber laser," Optics Letters 45, 5 (2019).
[18] Semaan, G., Komarov, A., Salhi, M., & Sanchez, F., "Study of a harmonic mode lock stability under external continuous-wave injection," Optics Communications, 387, 65-69 (2017).
[19] Ribenek, V. A., Stoliarov, D. A., Korobko, D. A., & Fotiadi, A. A., "Mitigation of the supermode noise in a harmonically mode-locked ring fiber laser using optical injection," Optics Letters, 46(22), 5747-5750 (2021).
[20] Korobko, D. A., Ribenek, V. A., Stoliarov, D. A., Mégret, P., & Fotiadi, A. A., "Resonantly induced mitigation of supermode noise in a harmonically mode-locked fiber laser: revealing the underlying mechanisms," Optics Express, 30(10), 17243-17258 (2022).
[21] Komarov, A., Komarov, K., Niang, A., and Sanchez, F., "Nature of soliton interaction in fiber lasers with continuous external optical injection," Physical Review A 89, 013833 (2014).
[22] Niang, A., Amrani, F., Salhi, M., Leblond, H., Komarov, A., and Sanchez, F., "Harmonic mode-locking in a fiber laser through continuous external optical injection," Optics Communications 312, 1-6 (2014).
[23] Ribenek, V. A., Stoliarov, D. A., Korobko, D. A., & Fotiadi, A. A., "Pulse repetition rate tuning of a harmonically mode-locked ring fiber laser using resonant optical injection," Optics Letters, 46(22), 5687-5690 (2021).
[24] Korobko, D. A., Ribenek, V. A., Itrin, P. A., Fotiadi, A. A., "Birth and annihilation of solitons in harmonically mode-locked fiber laser cavity through continuous wave injection," Optical Fiber Technology, 75, 103216 (2023).
[25] Liu, X., "Hysteresis phenomena and multipulse formation of a dissipative system in a passively mode-locked fiber laser," Physical Review A, 81(2), 023811 (2010).
[26] Tang, D. Y., Zhao, L. M., Zhao, B., & Liu, A. Q., "Mechanism of multisoliton formation and soliton energy quantization in passively mode-locked fiber lasers," *Physical Review A*, *72*(4), 043816 (2005).
[27] Korobko, D. A., Okhotnikov, O. G., & Zolotovskii, I. O. (2015). Long-range soliton interactions through gain-absorption depletion and recovery. Optics letters, 40(12), 2862-2865.
[28] Kutz, J. N., Collings, B. C., Bergman, K., & Knox, W. H., "Stabilized pulse spacing in soliton lasers due to gain depletion and recovery," IEEE journal of quantum electronics, 34(9), 1749-1757 (1998).
[29] Gumenyuk, R., Okhotnikova, E. O., Philippov, V. N., Korobko, D. A., Zolotovskii, I. O. and Guina, M., "Fiber Lasers of Prof. Okhotnikov: Review of the main achievements and breakthrough technologies," IEEE Journal of Selected Topics in Quantum Electronics 24(3), 1–14 (2018).
[30] Schröder, J., Alasia, D., Sylvestre, T., & Coen, S., "Dynamics of an ultrahigh-repetition-rate passively mode-locked Raman fiber laser," JOSA B, 25(7), 1178-1186 (2008).
[31] Korobko, D. A., Stoliarov, D. A., Itrin, P. A., Ribenek, V. A., Odnoblyudov, M. A., Petrov, A. B., & Gumenyuk, R. V. (2021). Stabilization of a harmonic mode-locking by shifting the carrier frequency. Journal of Lightwave Technology, 39(9), 2980-2987.
[32] Man, W. S., Tam, H. Y., Demokan, M. S., Wai, P. K. A., & Tang, D. Y., "Mechanism of intrinsic wavelength tuning and sideband asymmetry in a passively mode-locked soliton fiber ring laser," JOSA B, 17(1), 28-33 (2000).
[33] Akhmediev, N., Soto-Crespo, J. M., & Town, G., "Pulsating solitons, chaotic solitons, period doubling, and pulse coexistence in mode-locked lasers: Complex Ginzburg-Landau equation approach," Physical Review E, 63(5), 056602 (2001).
[34] Zhao, L. M., Tang, D. Y., Lin, F., & Zhao, B., "Observation of period-doubling bifurcations in a femtosecond fiber soliton laser with dispersion management cavity," Optics express, 12(19), 4573-4578 (2004).

[35] Chen, H. J., Tan, Y. J., Long, J. G., Chen, W. C., Hong, W. Y., Cui, H., & Xu, W. C., "Dynamical diversity of pulsating solitons in a fiber laser," Optics express, 27(20), 28507-28522 (2019).
[36] Wei, Z. W., Liu, M., Ming, S. X., Luo, A. P., Xu, W. C., & Luo, Z. C., "Pulsating soliton with chaotic behavior in a fiber laser," Optics letters, 43(24), 5965-5968 (2018).
[37] Liu, X., Närhi, M., Korobko, D., & Gumenyuk, R. "Amplifier similariton fiber laser with a hybrid-mode-locking technique," Optics Express, 29(22), 34977-34985 (2021).
[38] Ma, X., Zhang, K., Li, C., Chen, K., Zhou, Y., Zhang, W., & Gao, W., "Decaying dynamics of harmonic mode-locking in a SESAM-based mode-locked fiber laser," Optics Express, 31(22), 36350-36358 (2023).
[39] Pu, G., Zhang, L., Hu, W., & Yi, L., "Automatic mode-locking fiber lasers: progress and perspectives," Science China information sciences, 63, 1-24 (2020).
[40] Yan, X., Jiang, M., Li, E., Kang, X., Ren, Z., Li, D.,& Lu, B. "Tunable high-order harmonic and dual-wavelength mode-locking in Er-doped fiber laser based on Ti3C2T x-Mxene," Applied Physics Express, 14(1), 012009 (2021).